Effect of Geoacoustic Parameters Uncertainties on Acoustic Transmission Loss Prediction

GAO WEI
Yichang Testing Technology Research Institute
No. 555 Box, Yichang, Hubei Province 443003
People's Republic of China
wellgao2003@163.com

Abstract: - Geoacoustic parameters inverted from reverberation vertical correlation (RVC) are often directly used to predict the acoustic transmission loss (ATL) in shallow water. However, little work has been applied to the problem of quantifying uncertainty in predicted ATL produced by geoacoustic parameters uncertainties. In this paper, a posterior predictive probability analysis method (PPPAM) is first employed to evaluate the effects of geoacoustic parameters uncertainties inverted from RVC data on both coherent and incoherent ATL predictions. Where, the geoacoustic parameters uncertainties are characterized by their posterior probability distributions (PPD). And then the uncertainties of ATL prediction are analyzed quantitatively based on the posterior predictive probability distributions of ATL, which are the function of the PPDs of geoacoustic parameters and can be estimated using a Markov Chain Monte Carlo sampling method. Finally, the Yellow Sea Reverberation experimental results illustrate the PPPAM and show that: (1) in the range from 1km to 5 km, the mean values of 90% posterior credibility intervals (PCI) of coherent and incoherent ATL in frequency range of 500~800Hz exceed 6dB and 3dB, respectively; (2) the coherent ATL are more difficult to predict near the positions of destructive interference of the normal modes. These results derived in this paper are helpful to evaluate and improve the detection and localization performance of sonar system.

Key-Words: - Transmission loss prediction, Uncertainty analysis, Geoacoustic inversion, Posterior predictive probability, Reverberation vertical correlation.

1 Introduction

Geoacoustic parameters, including the sea-bottom velocity, density and attenuation, are very important for the acoustic transmission loss (ATL) prediction in shallow water. Thus, how to obtain the accurate geoacoustic parameters is one of the key issues in ATL prediction. In the past 20 years, the acoustic inversion techniques have been proved to be the most efficient and popular way to estimate geoacoustic parameters, particularly for those that are difficult to measure using the direct geophysical sampling method (i.e. gravity sampling core) [1]. Many studies have shown that unknown geoacoustic parameters can be inverted from different data types: acoustic transmission data [2], reverberation loss data [3], reverberation vertical correlation (RVC) data [4-6], ship self-noise [7], etc. However, the inversion results of geoacoustic parameters based on each of these data types may present some degrees of uncertainties due to the effects of theoretical model simplification and observed noise [8-11]. If the geoacoustic inversion results are directly used to calculate the ATL using a numerical acoustic propagation model, the ATL prediction will be affected by this uncertainty [12].

Recently, the above problem of quantifying the uncertainties in predicted ATL produced by geoacoustic parameters uncertainties has received much attention. Refs. [13] and [14] proposed an analytical method to describe the uncertainties of ATL prediction, respectively. The disadvantage of these methods is that they are only used to solve the simple problems. Refs. [15] and [16] then presented a numerical analysis method based on Bayesian interference to quantify the uncertainties of *coherent* ATL prediction in the presence of geoacoustic parameters uncertainties in matched-field inversion (MFI). One of the limitations of these studies is that they did not consider the case of *incoherent* ATL prediction in advance. But in fact, many researchers have pointed out that someplace the *incoherent* ATL prediction is more useful than *coherent* ATL prediction, especially in a complicated environment. Furthermore, the main conclusions presented in Refs.[15] and [16] are only proper to the problem of MFI. MFI is considered as an effective but expensive method for geoacoustic inversion. So in many cases, the geoacoustic parameters are often inverted from other data types (such as RVC data) and then used to predict ATL. In contrast to MFI, the obvious advantage of using RVC for geoacoustic inversion is quick and inexpensive because all of the required data can be obtained from only one ship for the experiment. In recent years, the RVC inversion technique has been developed by many authors and the uncertainties of geoacoustic inversion results have also analyzed in detail [3-6]. However, for the RVC inversion problem, few works have examined the effects of geoacoustic inversion uncertainties on the ATL prediction.

The main objective of this study was to investigate the effects of geoacoustic parameters uncertainties inverted from experimental RVC data on the both coherent and incoherent ATL prediction. First, based on the RVC data acquired from the Yellow Sea Reverberation Experiment 2005 (YSRE2005), the uncertainties of geoacoustic parameters inversion results are characterized by their posterior probability distributions (PPDs) in this paper. Then a posterior predictive probability analysis method is first used to evaluate the effects of geoacoustic inversion uncertainties on ATL prediction in the frequency range from 500Hz to 800Hz. To the author's knowledge, the similar work has not been reported in the literature.

The remainder of this paper is organized as follows. Section 2 briefly describes the basic formulas of the posterior probability analysis method, which can be used to quantify the uncertainties of geoacoustic inversion results. In section 3, the posterior predictive probability analysis method and the corresponding numerical integration technique are introduced. Section 4 describes the Yellow Sea reverberation experiment 2001 and then applies the posterior predictive probability analysis method to the experimental RVC data with the goal of evaluating the effects of geacounstic parameters uncertainties on ATL prediction. Finally, the results of this work are summarized and discussed.

2 Posterior probability distributions for geoacoustic parameters

The RVC inversion technique is widely applied to estimate the geoacoustic parameters [4-6]. The basic principle of the RVC inversion technique is to estimate the unknown geoacoustic parameters $\boldsymbol{m} = \begin{bmatrix} m_1 & m_2 & \cdots & m_N \end{bmatrix}$ by minimizing a misfit function $\phi(\boldsymbol{m})$ via nonlinear optimization method, such as Simulated Annealing, Genetic Algorithm, and hybrid inversion algorithms. Where $\phi(\boldsymbol{m})$ quantifies the mismatch between the observed RVC and the theoretical RVC, N is the number of unknown parameters. The best estimates for the unknown parameters then correspond to the lowest mismatch. However, because of the ambiguity imposed by a variety of factors, including unavoidable observed noise and theoretical simplifications of RVC model, the parameters inversion result using the technique above may present some degrees of uncertainties.

From the viewpoint of Bayesian inverse theory, the uncertainties of geoacoustic parameters can be estimated by their posterior probability density (PPD) [17]. The PPDs combines prior information about the model with the information provided by an observed data set. Let $\boldsymbol{C}$ and $\boldsymbol{m}$ represent the observed RVC data and the unknown geoacoustic parameters, the PPDs of $\boldsymbol{m}$ given $\boldsymbol{C}$ may be expressed as the following conditional probability distribution

$$p(\boldsymbol{m}|\boldsymbol{C}) \propto L(\boldsymbol{m})\, p(\boldsymbol{m}) \tag{1}$$

when normalized, then

$$p(\boldsymbol{m}|\boldsymbol{C}) = \frac{L(\boldsymbol{m})\, p(\boldsymbol{m})}{\int L(\boldsymbol{m})\, p(\boldsymbol{m}')\, d\boldsymbol{m}'} \tag{2}$$

where, $p(\boldsymbol{m})$ is the prior probability distribution. The likelihood function $L(\boldsymbol{m})$ is determined by the form of the data and the statistical distribution of the data errors, including both observed and theoretical error. In practical cases, the data error is often assumed Gaussian distributed, second-order stationary with zero mean and diagonal covariance matrix $v\boldsymbol{I}$ [18]. Under this assumption, the likelihood function satisfies

$$L(\boldsymbol{m}) \propto \exp\left[-E(\boldsymbol{m})\right] \tag{3}$$

where $E(\boldsymbol{m})$ is the error function appropriate to the state of available function. For RVC inversion problem, the error function can be described by

$$E(\boldsymbol{m}) = \sum_{f=1}^{F} \frac{\phi(\boldsymbol{m})}{v_f} \tag{4}$$

where $\phi(\boldsymbol{m}) = \left|\boldsymbol{C}_f(\boldsymbol{m}) - \boldsymbol{C}_f\right|^2$ is the misfit function [6], f is the frequency which is selected to invert the geoacoustic parameters. F is the number of the selected frequencies. $\boldsymbol{C}$ and $\boldsymbol{C}(\boldsymbol{m})$ are the observed and theoretical values of RVC, respectively. The data variance at the fth frequency can be estimated by solving $\frac{\partial L}{\partial v_f} = 0$

$$v_f = \phi(\hat{\boldsymbol{m}}) = \left|\boldsymbol{C}_f(\hat{\boldsymbol{m}}) - \boldsymbol{C}_f\right|^2 \tag{5}$$

where $\hat{\boldsymbol{m}}$ is the maximum a posterior solution, which corresponds to the minimum value of the misfit function.

If the bottom scattering coefficient is assumed to satisfy the Lambert scattering law, the normal-mode model of RVC between two different receivers can be expressed as [19]

$$\boldsymbol{C}(\boldsymbol{m}) = \left[C_{t_1}(\boldsymbol{m})\ C_{t_2}(\boldsymbol{m}) \cdots C_{t_N}(\boldsymbol{m})\right] \tag{6}$$

where

$$\begin{aligned} C_t(\boldsymbol{m}) &= \sum_n \left[\frac{\Phi_n(z_{r1}) A_n^2(h) \Phi_n(z_{r2})}{\sin(\alpha_n) \mathrm{e}^{-2\beta_n r} (\mu_n)^{-1}}\right] \\ &\times \left\{\sum_n \left[\frac{\Phi_n^2(z_{r1}) A_n^2(h)}{\sin(\alpha_n) \mathrm{e}^{-2\beta_n r} (\mu_n)^{-1}}\right]\right\}^{-\frac{1}{2}} \\ &\times \left\{\sum_n \left[\frac{\Phi_n^2(z_{r2}) A_n^2(h)}{\sin(\alpha_n) \mathrm{e}^{-2\beta_m r} (\mu_n)^{-1}}\right]\right\}^{-\frac{1}{2}} \end{aligned} \tag{7}$$

where z_{r1} and z_{r2} are the depth of receivers. $\Phi_n(z)$ stands for the nth normal mode functions, μ_n and β_n represent the horizontal wavenumber of mode and the mode attenuation, respectively. $A_n(h)$ denotes the amplitude of the mode function, h is the water depth, $r = ct/2$, c is the average velocity of sea water, t is the reverberation time. α_n is the incident angle of nth normal mode.

The 1-D marginal PPD for the ith parameter in the model vector $\boldsymbol{m}$ is defined as

$$P(m_i|\boldsymbol{d}) = \int_M \delta(m_i' - m_i)\, p(\boldsymbol{m}'|\boldsymbol{d})\, d\boldsymbol{m}' \tag{8}$$

where δ represents the Dirac delta function and M is the domain of integration which spans the multi-dimensional model space. The 1-D marginal PPD is considered as the most important moment in quantifying the uncertainties of unknown geoacoustic parameters [17].

3 Posterior predictive probability for transmission loss

In most cases, the geoacoustic parameters inversion results are often directly used to predict the transmission loss. Then the uncertainties of geoacoustic parameters are also mapped into the predicted ATL via the acoustic propagation model. To address this uncertainty of ATL prediction, the fundamental equation and the corresponding numerical integration technique of posterior predictive probability of ATL will be presented in this section.

3.1 Fundamental equation

For given range and given depth, the posterior predictive probability $p(u|\boldsymbol{C})$ of ATL u given $\boldsymbol{C}$ is obtained from [16]

$$p(u|\boldsymbol{C}) = \int_M p(u|\boldsymbol{m})\, p(\boldsymbol{m}|\boldsymbol{C})\, d\boldsymbol{m} \tag{9}$$

where $p(\boldsymbol{m}|\boldsymbol{C})$ is the PPD of geoacoustic parameter (see section 2), the conditional probability distribution $p(u|\boldsymbol{m})$ satisfies:

$$p(u|\boldsymbol{m}) = \delta(U(\boldsymbol{m}) - u) \tag{10}$$

where $U(\boldsymbol{m})$ is the predicted ATL via an acoustic propagation model. The mapping between geoacoustic parameters $\boldsymbol{m}$ and ATL U is assumed deterministic. Substitute Eq.(9) into Eq.(8), we may obtain the analytical expression of posterior predictive probability of ATL

$$p(u|\boldsymbol{C}) = \int_M \delta(U(\boldsymbol{m}) - u)\, p(\boldsymbol{m}|\boldsymbol{C})\, d\boldsymbol{m} \tag{11}$$

Eq.(11) not only describes the functional relationship between uncertainties of the inverted geoacoustic parameter and that of the predicted ATL, but also can be used to quantify uncertainties in predicted ATL produced by inverted parameters uncertainties. But in general, there is not an analytical method to estimate the multi-dimensional integrals of Eq.(11), which is typically carried out using a numerical integration technique. In the following subsection, an efficient numerical method based on Metropolis-Hasting algorithm will be presented.

3.2 Markov Chain Monte Carlo sampling

Markov Chain Monte Carlo (MCMC) sampling method is based on an analogy with thermodynamic processes as described by statistical mechanics [20]. The most common application of MCMC is numerical calculating multi-dimensional integrals. In this paper, MCMC is used to obtain the unbiased sampling of posterior predictive probability of ATL. A briefly summary of the steps needed in MCMC sampling method outlines here.

Step 1: Determine the search space of unknown geoacoustic parameters based upon the prior information; select an appropriate misfit function $\phi(\boldsymbol{m})$ and an optimization algorithm.

Step 2: Apply the optimization algorithm to minimize the misfit function and then obtain the maximum a posterior solution $\hat{\boldsymbol{m}}$. Substitute $\hat{\boldsymbol{m}}$ into Eq.(5) and we may obtain the value of the data variance v .

Step 3: $\hat{\boldsymbol{m}}$ is set as the starting point of MCMC sampling processing. And the number of criteria i equals to 1.

Step 4: Generate a new candidate point $\boldsymbol{m}'$ from a proposal distribution $q(\boldsymbol{m}'|\boldsymbol{m})$. For simplicity, the most common $q(\boldsymbol{m}'|\boldsymbol{m})$ used in practice is the symmetric distributions, such as the uniform distribution and the Gaussian distribution.

Step 5: Compute the acceptance probability α according to the following expression

$$\alpha = \min\left\{1, \frac{p(\boldsymbol{m}'|\boldsymbol{C})\, q(\boldsymbol{m}_i|\boldsymbol{m}')}{p(\boldsymbol{m}_i|\boldsymbol{C})\, q(\boldsymbol{m}'|\boldsymbol{m}_i)}\right\} \tag{12}$$

where $p(\ )$ represents the PPD of $\boldsymbol{m}$.

Step 6: Generate a random number $a \in [0,1]$ uniformly. If the acceptance probability $\alpha > a$, then the candidate point is accepted ($\boldsymbol{m}_{i+1} = \boldsymbol{m}'$). Otherwise $\boldsymbol{m}_{i+1} = \boldsymbol{m}_i$.

Step 7: Repeat step 4-6 above until the convergence of the estimated PPD have been verified. A popular MCMC convergence criterion is that the maximum difference between the cumulative marginal distributions for all parameters estimated from two runs in parallel is less than a prescribe threshold ε . Mathematically, this convergence criterion can be expressed as:

$$\max\left[\left|p_1\left(m_j\middle|\boldsymbol{C}\right) - p_2\left(m_j\middle|\boldsymbol{C}\right)\right|\right] < \varepsilon \tag{13}$$

where $p(m_j|\boldsymbol{C})$ is the marginal PPD of the jth parameter in $\boldsymbol{m}$ given $\boldsymbol{C}$.

Step 8: The program is terminated. And all samples during MCMC sampling procedure are used to calculate the PPDs of unknown parameters in terms of the following expression

$$p(\boldsymbol{m}|\boldsymbol{C}) = \frac{\sum_{k=1}^{Q} \delta(\boldsymbol{m}_k - \boldsymbol{m})}{Q} \tag{14}$$

According to Eq.(9), (10, (13)) and (14), the posterior predictive probability of u for a set of discrete ranges and depths given the observed RVC data $\boldsymbol{C}$ can be computed by

$$p(u|\boldsymbol{C}) = \frac{\sum_{k=1}^{Q} \delta(U(\boldsymbol{m}_k) - u)}{Q} \tag{15}$$

where, Q denotes the total number of sample points.

4 Experimental results and discussion

4.1 Reverberation experiment

A reverberation experiment was conducted in shallow water with a depth of 36.25m on 22:46:23 September 8, 2005 at a site in the Yellow Sea, centred at 121°21.11'E □ 35°15.00'N. Explosive sources with 50-g TNT were used as sound sources in the experiment, and the source depth is around 25 m. The sound speed profile in the water column, measured by conductivity temperature depth (CTD), is shown in Fig.1. Two receivers were located at depths of 18.9m and 21.9m. Fig. 2 shows the shallow water reverberation time series obtained by the 18.9 m receiver and the sampling frequency was 12 KHz. Then the experimental RVC between two receivers for reverberation time t and centre frequency f can be calculated by

$$\boldsymbol{C}_f = \left[\sum_{t-\Delta t/2}^{t+\Delta t/2} \left| p_1(t)\, p_2(t) \right| \right] \times \left[\sqrt{ \sum_{t-\Delta t/2}^{t+\Delta t/2} \left| p_1(t) \right|^2 \sum_{t-\Delta t/2}^{t+\Delta t/2} \left| p_2(t) \right|^2 } \right]^{-1} \tag{16}$$

where p_1 and p_2 are the reverberation data received by two different receivers, respectively. For inversion, the experimental area is characterized by a fair flat bottom. And the sea bottom is modelled as a half infinite space with the uniform sound velocity, density and attenuation. Then the sea bottom sound velocity c, density ρ and attenuation α_f for all frequencies are the unknown parameters that are to be inverted from the RVC data. Moreover, the Multi-frequency hybrid inversion scheme is used to invert the geoacoustic parameters in this analysis, where the frequencies selected to the inversion include 500, 600, 700 and 800Hz.

4.2 Geoacoustic inversion result

In this subsection, the PPDs of unknown geoacoustic parameters based on RVC data obtained during the reverberation experiment above will be reported and be used to analyze the uncertainties of the geoacoustic inversion results. To estimate the PPDs of unknown parameters, Genetic Algorithm (GA) is applied to obtain the maximum a posterior solution and the data variance v during MCMC sampling procedure (see step 1 and 2 in subsection 2.2). GA is adaptive heuristic search algorithm premised on the evolutionary ideas of natural selection and genetic. The complete description of GA is documented in [21].The values of GA parameters in this study are as follows: the population size was set to 64; reproduction size was 0.5; crossover probability was 0.8; mutation probability was 0.08; the generation of GA was 200.

The 1-D marginal PPD for the six parameters are shown in Fig.3. The horizontal axes show the search spaces, the vertical axes indicate the posterior probabilities, and the vertical dashed lines are positions corresponding to the optimum values (i.e. maximum a posterior solution) of each parameter. It can be seen from Fig.3 that for the sea bottom sound velocity c and attenuation α, their PPDs all converge to the optimum values with high probabilities. On the other hand, the posterior probability of density ρ is lower near its optimum value. These results show that c and α are all well determined, but inversions for bottom density ρ are comparatively less reliable.

4.3 ATL prediction

According to the classical normal mode theory [22], the coherent acoustic transmission loss (ATL) $u(R,D,\boldsymbol{m})$ at a depth D and range R in an environment may be expressed as

$$u(R,D,\boldsymbol{m}) = -20\log \left| \frac{1}{\rho(D_s)} \sqrt{\frac{2\pi}{R}} \sum_{n=1}^{\infty} \left\{ \frac{\Phi_n(D_s,\boldsymbol{m})\Phi_n(D,\boldsymbol{m}) \exp\left[ik_n(\boldsymbol{m})R\right]}{\sqrt{k_n(\boldsymbol{m})}} \right\} \right| \tag{17}$$

where Φ_n is the normal mode corresponding to the horizontal wave number k_n. D_s is the depth of source, ρ is the density of sea water. Eq. (17) is only suitable to the case of the coherent ATL. However, the incoherent ATL is also important for the problem of predicting acoustic transmission loss in many practical applications. Because the ocean environments are very complex and variable in both space and time, it is hard to predict or observe the coherent ATL associated with modal interference in some cases. Thus, the interference between the different modes is often neglected. The theoretical expression of incoherent ATL is given by [22]

$$u_{\text{Inc}}(R,D,\boldsymbol{m}) = -20\log \frac{1}{\rho(D_s)} \sqrt{\frac{2\pi}{R}} \sqrt{ \sum_{n=1}^{\infty} \left| \left\{ \frac{\Phi_n(D_s,\boldsymbol{m})\Phi_n(D,\boldsymbol{m}) \exp\left[ik_n(\boldsymbol{m})R\right]}{\sqrt{k_n(\boldsymbol{m})}} \right\} \right|^2 } \tag{18}$$

Obviously, the coherent and incoherent ATLs are all the function of the geoacoustic parameter $\boldsymbol{m}$. As long as $\boldsymbol{m}$ is known, the transmission loss as given by Eq. (17) or (18) may be calculated using any normal-mode code, such as KRAKEN [23] and MOATL [24]. That is to say, the transmission loss may be predicted at all frequencies, ranges and depths in the same geoacoustic environment.

Fig.4 shows the posterior predictive probabilities of coherent ATL for 500Hz and a source depth of

20m at different ranges (R =1.5, 2.5, 3.5 and 4.5km) and depths (D =15, 25 and 30m). The dashed lines are positions corresponding to the optimum values of coherent ATL prediction which are calculated using Eq.(17) based on the optimum geoacoustic parameters inverted from RVC data. It can be seen from Fig.4 that:

(i) At some positions $\left(D = 15\text{m}, R = 3.5\text{km}\right)$, $\left(D = 15\text{m}, R = 4.5\text{km}\right)$ and $\left(D = 25\text{m}, R = 3.5\text{km}\right)$, the posterior predictive probability distributions of coherent ATL are relative flat and can not converge to the optimum values with high probabilities. Moreover, it is observed that these positions all correspond to the local maximum values of coherent ATL, i.e. the points of modal destructive interference (see Fig.4 for detail). This result indicates that the modal destructive interference is more sensitive to the geoacoustic parameters uncertainties; it is more difficult to predict coherent ATL near the positions of destructive interference.

(ii) Depending on the measured results of sound speed profile using CTD, the thermocline depth at the experimental site ranges from about 22m to 27m (see Fig.1). It is found that the posterior predictive probabilities near the optimum values of predicted coherent ATL at D =30m (below the thermocline) are higher than the cases of D =15m (above the thermocline) and D =25m (in the thermocline) at the same range. That is to say, the uncertainties of coherent ATL prediction are relative small below the lower bound depth of thermocline. This phenomenon is not reported previously and might be explained by the fact that the coherent ATL below the thermocline is dominated by the low-order modes, which is not sensitive to the attenuation and less affected by the attenuation uncertainties.

Fig.5 shows the optimal values (dashed lines) and 90% posterior credibility intervals (PCI) of coherent ATL versus range for 500Hz at three different depths. In this paper, $x\%$ PCI is defined as the interval such that $x\%$ of the highest area of the posterior predictive probability is contained in this interval. The values of $x\%$ PCI are often used to quantify the uncertainties of ATL prediction. In general, the ATL prediction result with a small PCI is more reliable than a result with a large PCI. It can be seen from Fig.5 that the uncertainties of coherent ATL prediction are relative large: in the range from 1km to 5km, the maximum values and the mean values of 90% PCI exceed 20dB and 6dB, respectively.

Let us now consider the case of incoherent ATL prediction. Fig.6 shows the posterior predictive probabilities of incoherent ATL for 500Hz. In this figure, the ranges and the depths are the same as in Fig.4. The dashed lines correspond to the optimum values of predicted incoherent ATL. Fig.7 shows the optimum values (dashed lines) and 90% PCI of incoherent ATL versus range for 500Hz at different depth. It can be seen from Fig.6 and Fig.7 that the posterior predictive probability distributions of incoherent ATL may converge to the optimum values with high probabilities; the maximum values and the mean values of 90% PCI are less than 5dB and 3dB, respectively. The incoherent ATL can be well predicted based on the geoacoustic parameters inverted from RVC data. Furthermore, it can be seen form Fig.5 and Fig.7 that the uncertainties of the coherent and incoherent ATL prediction all increase with range increasing due to error accumulation effect.

This paper gets the similar conclusions above in the case of 600Hz, 700Hz and 800Hz.

5 Summary

In this paper, the uncertainties of geoacoustic parameters inverted from RVC data which collected during Yellow Sea Reverberation Experiment 2005 are analyzed based on the PPDs of geoacoustic inversion results. And then the effects of these parameters uncertainties on ATL prediction are investigated using the posterior predictive probability method. The main results obtained are summarized below:

(i) Near the positions of destructive interference of the normal modes, the posterior predictive probability distributions of coherence ATL are relative flat. This indicates that the maximum values of coherent ATL are more difficult to predict.

(ii) The degrees of uncertainties in coherent and incoherent ATL prediction vary with the depth of receiver. It is found that below the thermocline the coherent and incoherent ATL may be predicted with high accuracy. On the contrary, the geoacoustic parameters uncertainties have much more significant effects on the ATL prediction above (or in) the thermocline.

(iii) In the case of coherent ATL prediction, the maximum value and the mean value of 90% PCI in the range from 1km to 5 km exceed 20dB and 6dB, respectively. At the same conditions, the maximum values and the mean values of 90% PCI for incoherent ATL prediction are less than 5dB and

3dB. These results indicate that relative uncertainties in predicted incoherent ATL are small.

6 Acknowledge

The author would like to thank Institute of Acoustics, Chinese of Academy of Sciences and Harbin Engineering University for their coordination during the Yellow Sea Experiment 2005.

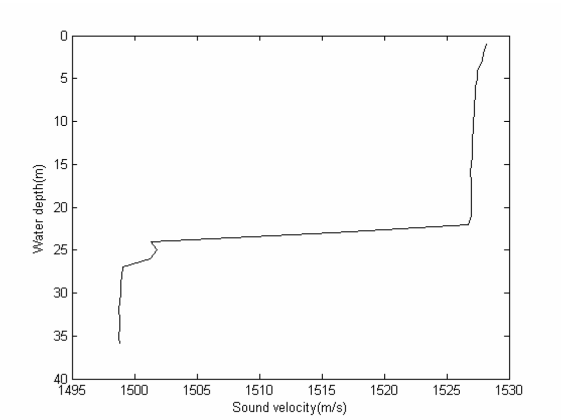

Fig. 1. Sound velocity profile during reverberation experiment

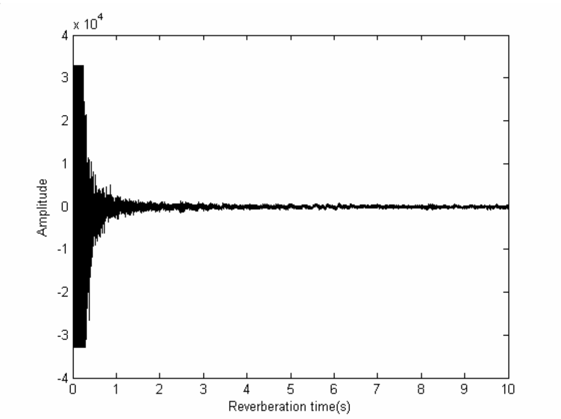

Fig. 2. Shallow water reverberation time series. Receiver depth=18.9m

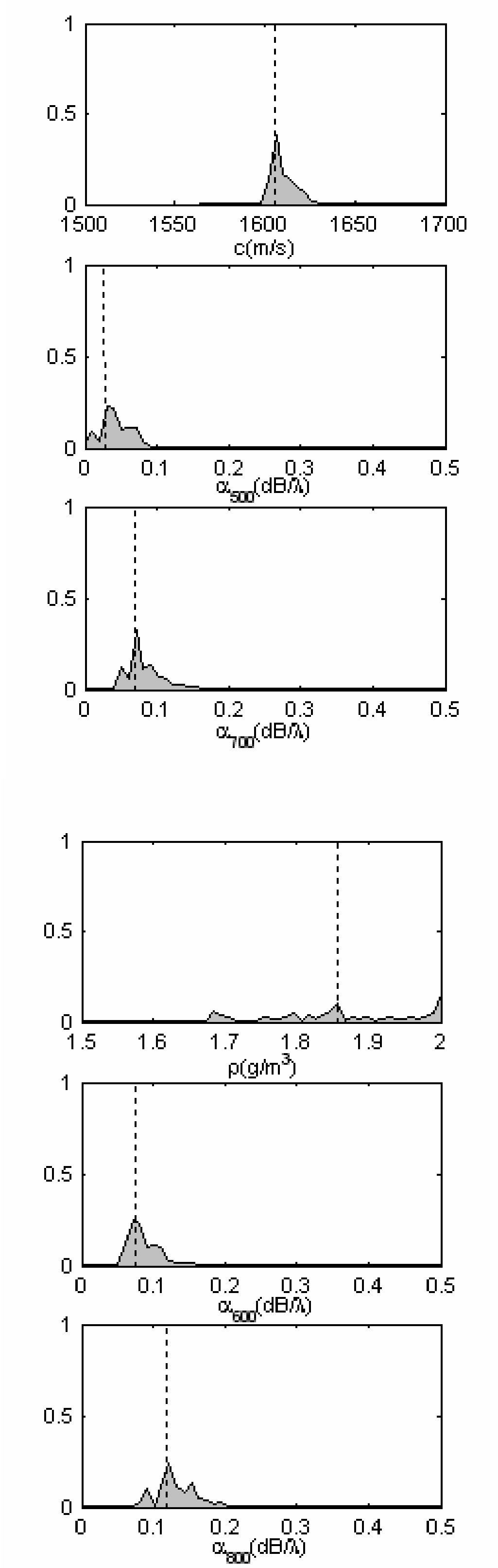

Fig. 3. 1-D marginal posterior probability distributions (PPDs) of the geoacoustic parameters. The dashed lines are positions corresponding to optimal values of the parameters. The horizontal axes indicate the search bounds

References:

[1] M.I. Taroudakis, G.N. Makrakis, *Inverse Problems in Underwater Acoustics*, Springer, 2001.

[2] P. Gertoft, C.F. Mecklenbräuker, Ocean acoustic inversion with estimation of a posterior probability distributions, *Journal of the Acoustical Society of America*, Vol.104, No.2, 1998, pp. 808-819.

[3] J.J. Liu, F.H. Li, L.H. Guo, Vertical correlation of shallow-water reverberation and inversion for bottom reflection loss and bottom scattering strength, *Acta Acoustica*, Vol.29, No.1, 2004, pp. 49-56.

[4] Z.L. LI, R.H ZHANG, Geoacoustic inversion by MFP combined with vertical reflection coefficients and vertical correlation, *IEEE Journal of Oceanic Engeneering*, Vol.29, No.4, 2004, pp. 973-979.

[5] J.X. ZHOU, X.Z. ZHANG, P.H. Rogers, *et al*. Reverberation Vertical Coherence and Sea-Bottom Geoacoustic Inversion in Shallow Water, *IEEE Journal of Oceanic Engeneering,* Vol.29, No.4, 2004, pp. 988-999.

[6] W. GAO, N. WANG, H.Z. WANG, Statistical geoacoustic inversion from vertical correlation of shallow water reverberation, *Acta Acousica*, Vol.33, No.2, 2008, pp. 109-115.

[7] D.J. Battle, P. Gerstoft, W.S. Hodgkiss, *et al*. Bayesian model selection applied to self-noise geoacoustic inversion, *Journal of the Acoustical Society of America*, Vol.116, No.2, 2004, pp. 2043-2056.

[8] J.X. Zhou, X.Z. Zhang, Shallow-water reverberation level: measurement techniques and initial reference values, *IEEE Journal of Oceanic Engineering*, Vol.30, 2005, pp.832-842.

[9] Z.H. Peng, J.X. Zhou, R.H. Zhang, In-plane bistatic backward scattering from seabottom with random inhomogeneities sediment and rough interface, *Sci. China, Ser. G*, Vol.47, 2004, pp.702–716.

[10] W.A. Kuperman, F. Ingenito, Attenuation of the coherent component of sound propagating in shallow water with rough boundaries, *Journal of the Acoustical Society of America*, Vol.61, 1977, pp.1178–1187.

[11] J.X. Zhou, X.Z. Zhang, Z.H. Peng, et al, Sea surface effect on shallow-water reverberation, *Journal of the Acoustical Society of America*, Vol.121, No.1, 2007, pp.98-107.

[12] P.F.J. Lermusiaux, C.S. Chiu, A.R. Robinson, Modelling uncertainties in the prediction of the acoustic wavefield in a shelfbreak environment. *Proc. of the 5th International conference on theoretical and computational acoustics*, May 21-25, 2001. Beijing, China. 2002.

[13] K.R. James, D.R. Dowling, A probability density function method for acoustic field uncertainty analysis, *Journal of the Acoustical Society of America*, Vol.118, No.5, 2005, pp. 2802-2810.

[14] S. Finette, Embedding uncertainty into ocean acoustic propagation models, *Journal of the Acoustical Society of America*, Vol.117, No.3, 2005, pp: L997-L1000.

[15] P. Gerstoft, C.F. HUANG, W.S. Hodgkiss, Estimation of transmission loss in the presence of geoacoustic inversion uncertainty, *IEEE Journal of Oceanic Engineering*, Vol.31, No.2, 2006, pp. 299-307.

[16] C.F. HUANG, P. Gerstoft, W. S. Hodgkiss, Validation of statistical estimation of transmission loss in the presence of geoacoustic inversion uncertainty, *Journal of the Acoustical Society of America*, Vol.120, No.4, 2006, pp.1932-1941.

[17] A. Tarantola, Inverse Problem Theory: *Methods for Data Fitting and Model Parameter Estimation*, Elsevier, 1987.

[18] M.K. Sen, P.L Stoffa, Bayesian inference, Gibbs' sampler and uncertainty estimation in geophysical inversion, *Geophys. Prospect*, Vol.44, No.2, 1996, pp. 313-350.

[19] F.H. Li, J.J. Liu, The vertical coherence of shallow water reverberation, *Acta Acousica*, Vol.28, No.6, 2003, pp. 494-503.

[20] S. E. Dosso, Quantifying uncertainty in Geoacoustic inversion II. Application to broadband, shallow water data, *Journal of the Acoustical Society of America*, Vol.111, No.1, 2002, pp.143–159.

[21] X.P. Wang, L.M. Cao, *Genetic algorithm-theory, application and implementation*, Xi'an Jiaotong University Press, 2002.

[22] F.B. Jensen, W.A. Kuperman, M.B Porter, et al, *Computational Ocean Acoustics*, American Institute of Physics Press,1994.

[23] M.B. Porter, *The KRAKEN Normal Mode Program,* SACLANT Undersea Research Centre Press, 1991.

[24] F. Ingenito, S. Wolf, J. Miller, "Modal acoustic transmission loss (MOATL)", NRL Press, 1980.

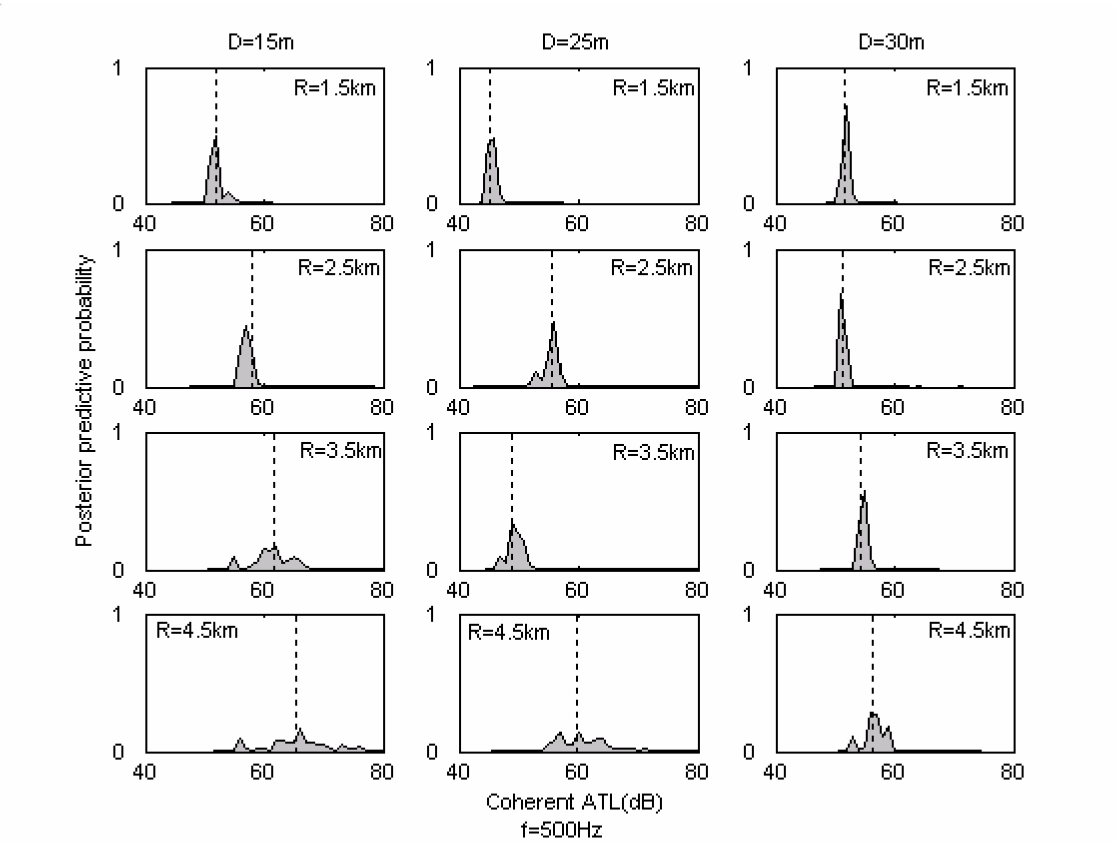

Fig. 4. Posterior predictive probability of coherent ATL at different range R and depth D. The dashed lines are positions corresponding to optimal values of coherence ATL

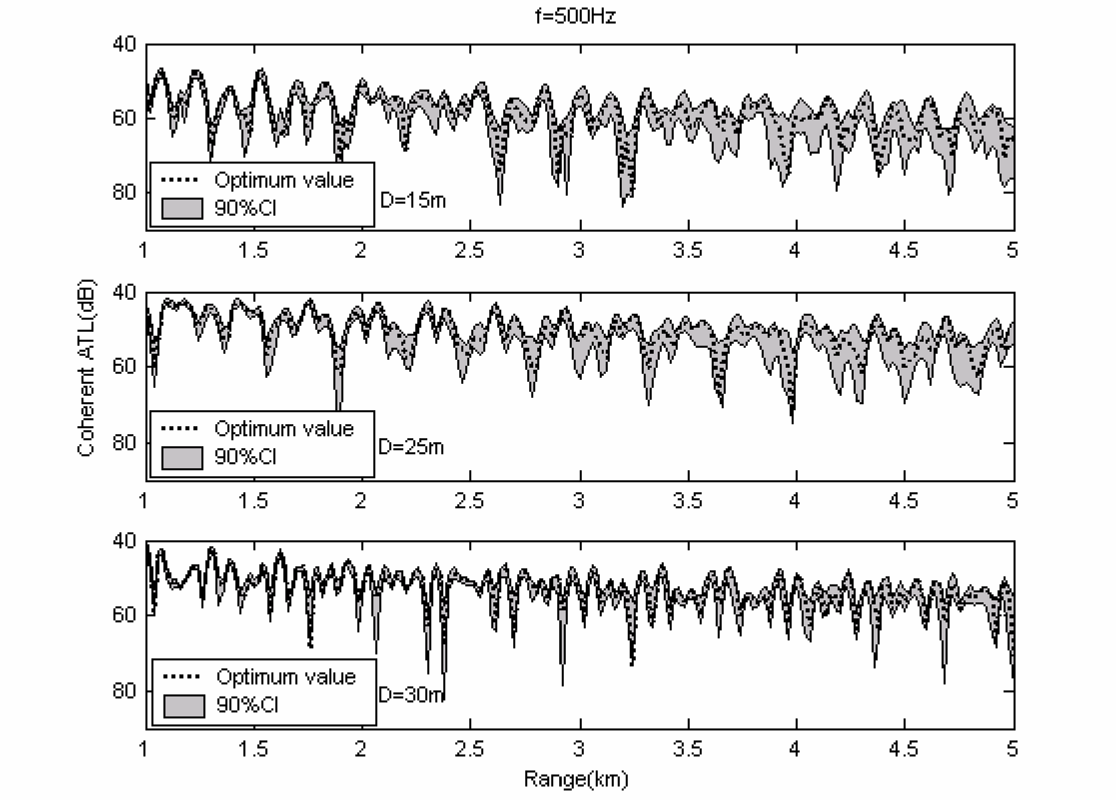

Fig. 5. The optimum values (dashed lines) and 90% posterior credibility intervals of coherent ATL versus range for 500Hz in the range from 1km to 5km.

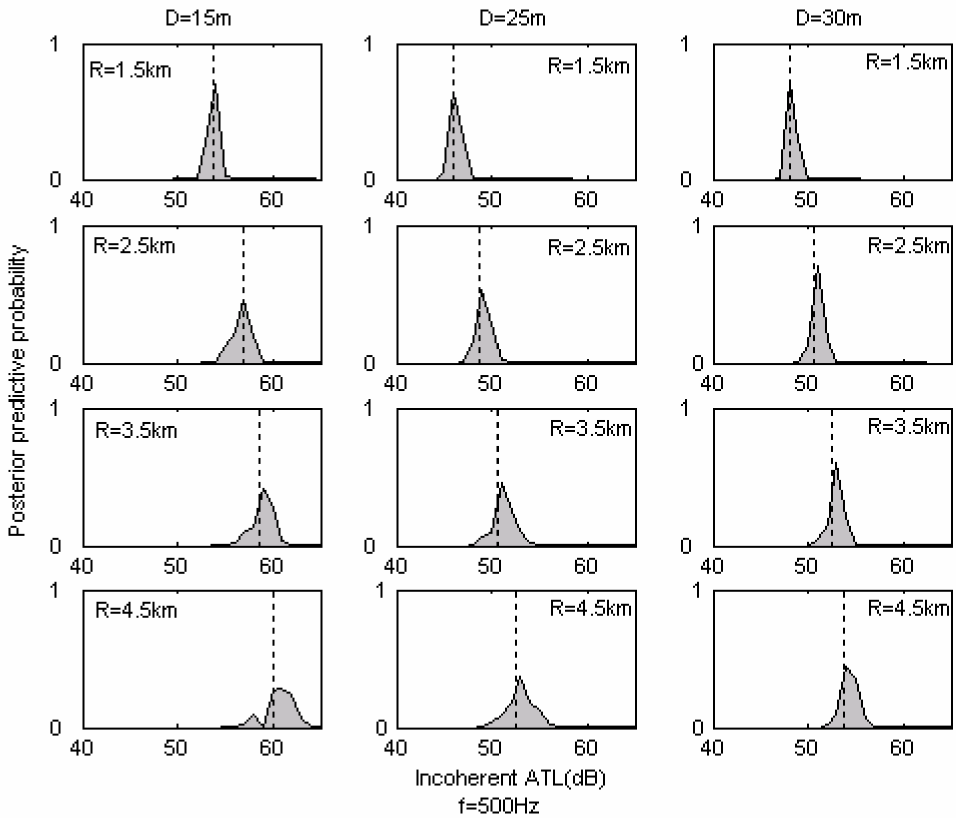

Fig. 6. Posterior predictive probability of incoherent ATL at different range R and depth D. The dashed lines are positions corresponding to optimal values of incoherent ATL

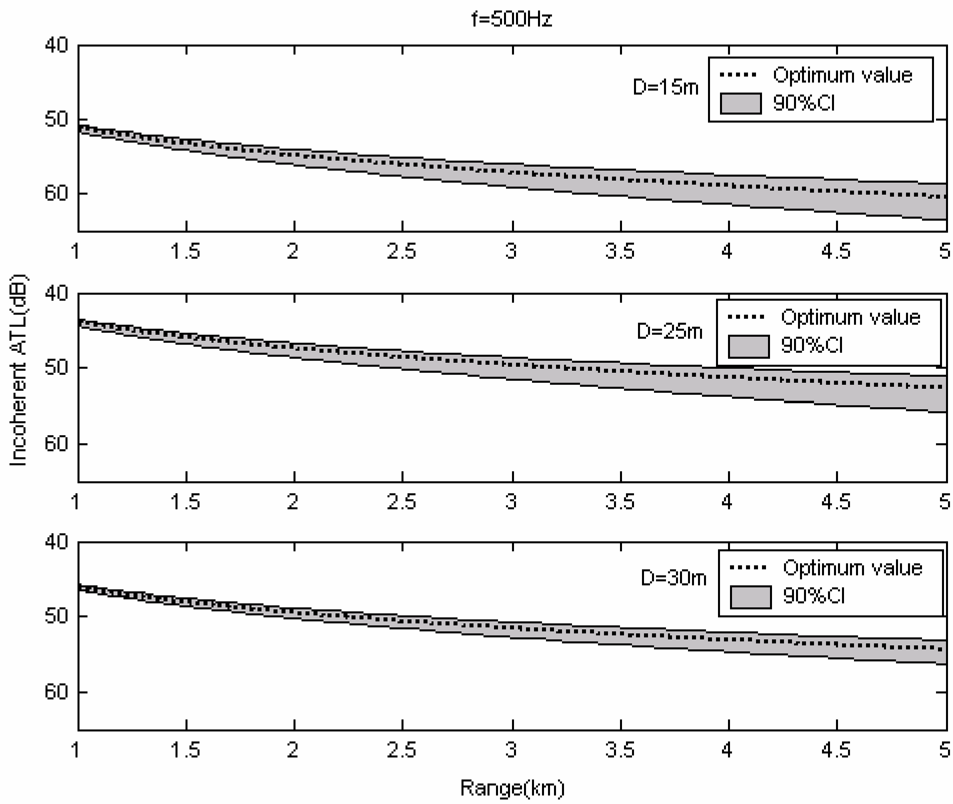

Fig. 7. The optimal values (dashed lines) and 90% posterior credibility intervals of incoherent ATL versus range for 500Hz in the range from 1km to 5km